PROCEEDINGS OF SCIENCE

Measurement of the mass composition of ultra-high-energy cosmic rays at the Pierre Auger Observatory

Eric Mayotte[a,*] **for the Pierre Auger Collaboration**[b]

[a] *Department of Physics, Colorado School of Mines, 1523 Illinois St., Golden CO, USA*
[b] *Observatorio Pierre Auger, Av. San Martín Norte 304, 5613 Malargüe, Argentina*
Full author list: https://www.auger.org/archive/authors_icrc_2023.html

E-mail: spokespersons@auger.org

After nearly 20 years of data-taking, the measurements made with the Pierre Auger Observatory represent the largest collection of ultra-high-energy cosmic ray (UHECR) data so far assembled from a single instrument. Exploring this data set led to a deeper understanding of the UHECR flux and many surprises. In particular, studies aiming to investigate and leverage the mass composition of UHECRs have played an important role in empowering discovery. This contribution will present an overview of the analyses of primary mass composition carried out during the first phase of the Observatory. The overview includes analyses derived from measurements made by the surface, fluorescence, and radio detectors covering energies ranging from 0.1 EeV up to 100 EeV. Special attention will be given to recent advances and results to provide a complete picture of UHECR mass composition at the Observatory as it moves to its next phase, AugerPrime. Additionally, specific updates will be given to studies focusing on mass trends from surface detector rise-times, $X_{\max}$ dependent anisotropies, and UHECR beam characterization using the correlation between $X_{\max}$ and signal amplitudes at the ground.

38th International Cosmic Ray Conference (ICRC2023)
26 July - 3 August 2023
Nagoya, Japan

*Speaker

PoS(ICRC2023)365

Phase-I of the Pierre Auger Observatory

The Pierre Auger Observatory has been observing ultra-high-energy cosmic ray (UHECR) air showers since Jan 1st, 2004 when data-taking began with 154 water-Cherenkov detectors (WCD) spaced at 1500 m and two partially completed fluorescence detector stations. The size of the Observatory then rapidly grew to its full extent. Since June 2008, it has been making precision measurements with 1600 WCD stations (the SD) and four fluorescence detector stations, each housing six fluorescence telescopes (the FD) [1]. Later, a three-telescope high-elevation angle FD extension (HEAT) and an infilled, 750 SD array were added to extend sensitivities to lower energies, and the 17 km^2 Auger Engineering Radio Array (AERA) was installed [2]. The Observatory then, more or less, remained in this configuration accumulating data through 2021 when the upgrade of the Observatory, Auger Prime [3], began to be deployed, changing the SD data. The data resulting from measurements of UHECR events made with the pre-upgrade instrumentation of the Observatory are referred to as the Phase-I dataset. This report focuses on the implications drawn on the mass composition of UHECRs thus far extracted from the analysis of the Phase-I dataset.

UHECR mass composition in Phase-I

A critical observation made during Phase-I of the Pierre Auger Observatory was that the mass composition of UHECRs strongly evolves with energy. The composition of the UHECR flux above 100 PeV can be generally described as follows. First, the vast majority of UHECR primaries are ionized atomic nuclei. Second, as energy increases, the mean mass of these nuclei first decreases, reaching its lightest point around 3 EeV, and then afterward, increases significantly. Third, over much of the energy range, evidence points to a UHECR flux best described as mixed in composition; however, above a few EeV, the flux continually increases in purity as energy climbs. These trends are robust, derived from a large variety of measurement techniques, strongly constrain possible acceleration and propagation scenarios, and are not dependent on hadronic interaction models.

The first indications of the above-described mass trends came from the measurements of the depth of shower maximum ($X_{\rm max}$) in 2010 using events simultaneously observed by the FD and SD (Hybrid events) [4]. Shower $X_{\rm max}$ is a compelling mass-sensitive observable as it is directly tied to the depth at which the first interaction of the UHECR primary particle occurred in the atmosphere, which naturally depends only on its cross-section and, therefore, in the case of atomic nuclei, its mass. This straightforward relationship means general mass trends can be extracted by looking at the energy evolution of the first two moments of $X_{\rm max}$ alone without relying on models. After this initial publication, the hybrid $X_{\rm max}$ analysis method was frequently updated [5–7], and $X_{\rm max}$ based analyses were developed for the SD array, AERA, and the low energy FD, HEAT. The most up-to-date summary of the latest $X_{\rm max}$ measurements made using FD [8], SD [9], AERA [10] and HEAT [6] is shown in Fig. 1, which clearly exhibits the above-described trends. There is an exceptional agreement between methods for $\langle X_{\rm max}\rangle$, despite a different $X_{\rm max}$ scale appearing in the FD, AERA, and SD/HEAT results due to progressive changes to reconstruction methods. There is some tension between the FD and SD in $\sigma\,(X_{\rm max})$, which may be due to residual model dependencies in the SD result or statistical effects in the FD result. The FD and SD measurements are of particular interest and are the subject of dedicated contribution in these proceedings ([8, 9]), which should be consulted for analysis details and expanded results.

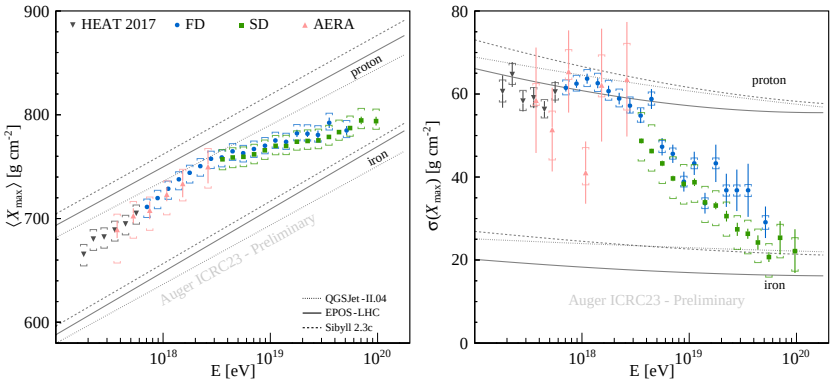

Figure 1: The first (left) and second (right) moments of $X_{\max}$ distributions measured with the FD [8], the SD [9], AERA [10], and HEAT [7] during Phase-I. Note: the systematic uncertainties on $\langle X_{\max} \rangle$ for the SD and FD are correlated.

Of the available techniques, the measurement of $X_{\max}$ using hybrid events delivers the highest resolution and lowest model dependence. However, it is also limited by the low uptime of the FD, $X_{\max}$ dependent aperture, and the need to correct for atmospheric conditions. As a result of this, hybrid measurements struggle with low statistics and relatively high systematics, limiting their power at energies above $10^{19.5}$ eV, an energy range critical to identifying astrophysical sources [11]. Statistics can be improved by deducing UHECR composition from SD data. However, unlike the FD, the SD can not directly observe the development of showers. Instead, SD methods must analyze the timing structure and distribution of particles arriving at the ground to extract signatures related to shower development and primary particle type. For example, a data-driven method used the mean risetime of signals from SD stations in an event (Δ) as it is related to the proximity of the shower maximum to the ground. By evaluating how the mean value of Δ evolved with energy, the mass trends seen in the Hybrid data were confirmed and extended to 100 EeV [12]. The most recent SD-only composition analysis applies machine-learning algorithms to the WCD signal traces collected to simultaneously leverage all SD information to estimate shower $X_{\max}$ directly, delivering a strong improvement over earlier techniques [9, 13]).

The direct measurement of $X_{\max}$, when combined with predictions from hadronic interaction models, allows for the straightforward calculation of the first two moments of the log of the mass of the primary particles ($\ln A$) making up the UHECR beam. An overview of the moments of $\ln A$ is shown in Fig. 2, which likewise shows impressive agreement between FD and SD-derived measurements. The plot of first moments ($\langle \ln A \rangle$) describes the energy evolution of the mean mass of primary cosmic rays and clearly shows the beam first becoming lighter before turning

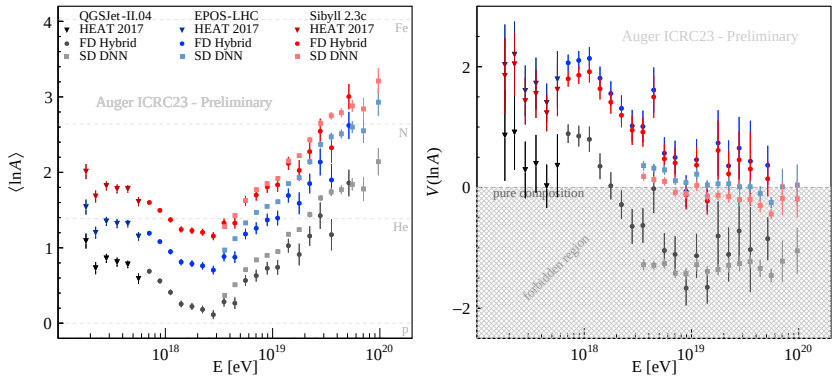

Figure 2: The first (left) and second (right) moments of $\ln A$ distributions derived from the FD and SD Phase-I $X_{\max}$ moments in Fig. 1 using QGSJet-II.04 (grey) [14], EPOS-LHC (blue) [15], and Sibyll 2.3c (red) [16].

around 3 EeV to becoming consistently heavier with energy for all hadronic models considered, with QGSJet-II.04 predicting the lightest composition and Sibyll 2.3c predicting the heaviest.

Interpretation of the second moments of $\ln A$, $V(\ln A)$, is more complex than the first moments. As energy increases, the beam moves from a regime of high mixing (values greater than zero) to one of higher beam purity (values around 0), with that change occurring a few energy bins higher than the 3 EeV minimum in mean primary mass. However, in both the FD and SD measurements derived using QGSJet-II.04, one will also notice that at an energy above $\sim$ 2 EeV, the variance of $\ln A$ crosses below the values associated with a pure composition into a forbidden regime. At these energies, the results of QGSJet-II.04 are unphysical. Its predictions are clearly in tension with observations, providing strong evidence that QGSJet-II.04 fails to adequately describe the fluctuations in $X_{\rm max}$ for real showers. As a result of this deficiency, it is recommended to only utilize this tool in situations where an inaccurate prediction of shower development will not adversely affect a study.

Obtaining a precise description of the UHECR beam beyond general patterns is challenging due to varied predictions of both $\langle \ln A \rangle$ and $V(\ln A)$ for different hadronic interaction models. Therefore, it is crucial to identify parameters that can provide model-independent probes of UHECR composition. One such parameter is the degree of correlation (r_G) between $X_{\rm max}$ and the signal in WCDs at 1000 m from the core corrected for zenith angle (S_{38}). This correlation is valuable as, in a mixed beam, the heavier nuclei will produce more muons than light nuclei leading to higher S_{38} values while also having shallower $X_{\rm max}$ values leading to negative r_G values. In pure beams, however, non-negative correlations are found in simulations. The top panel of Fig. 3 shows the energy evolution of r_G seen in data with model-derived expectations for pure and mixed compositions for comparison. The correlation remains significantly negative (6.4σ from zero) below the ankle, becoming compatible with zero and, therefore, less mixed compositions at higher energies. The bottom panel of Fig. 3, which demonstrates the expected correlation for beams with different mean masses and degrees of mixing (generated with Sibyll 2.3c) with the correlations seen in hybrid data indicated, provides a quantitative interpretation of this observation. The negative values observed below the ankle are compatible only to mixes with $\sigma(\ln A) > 1.0$ providing us with the hadronic interaction model-independent [7] evidence for a primary mix containing nuclei heavier than helium (for the maximum p-He mixing $\sigma(\ln A) \approx 0.7$).

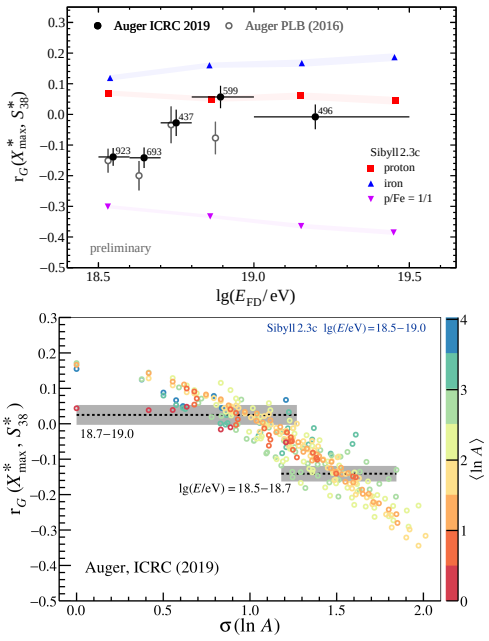

Figure 3: $S_{38}/X_{\rm max}$ correlation from hybrid data. The * in S^*_{38} and $X^*_{\rm max}$ denotes normalization to 10 EeV.

A powerful additional interpretation of the $X_{\rm max}$ data is possible by fully embracing model dependencies. Specifically, the observed distributions of $X_{\rm max}$ can be fit with model-generated templates of different primary mass groups to estimate how much each group contributes to the overall flux. From the results of this process, shown in Fig. 4, several conclusions can be drawn. First iron is almost entirely absent from the flux between $10^{18.4}$ eV and $10^{19.4}$ eV. Second, protons are a minor component above the ankle and become rare at the highest energies. Third, there

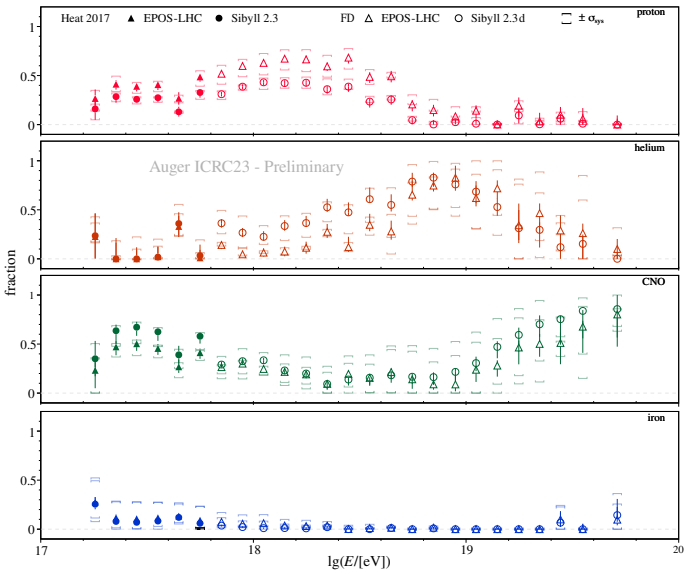

Figure 4: Fits of the fractional mass composition of the UHECR flux derived from HEAT [6] and FD [8] $X_{\max}$ data [17]. To extract the fractions, parameterizations of the anticipated $X_{\max}$ distributions for p, He, CNO, and Fe-generated using Sibyll 2.3 (HEAT), Sibyll2.3d, and Epos-LHC- are fit to the observed distributions of $X_{\max}$. QGSJet-II.04 has been omitted from this analysis due to its generally unphysical predictions. See [17] for detailed results, interpretations, and applications.

appears to be significant mixing in adjoining mass groups at all but the highest energies. Despite the reliance on models, the fractional fit approach is an effective technique for understanding the flux and generating a critical dataset for astrophysical modeling. As such, the methodology and results for these fraction fits are explored further in a dedicated contribution in these proceedings [17].

Update on the correlation between $X_{\max}$ and the galactic plane

Previous studies [18, 19] showed that there is an indication for a difference in the mean composition of UHECRs arriving within 30° of the galactic plane (on-plane) as compared to those arriving farther from it (off-plane) in the hybrid data. Since those reports, the process of reconstructing the longitudinal shower profile [20], the corrections for the aerosol content of the atmosphere [21], and the $X_{\max}$ analysis itself [8] have all undergone significant changes. In addition, the dataset has been expanded by adding three more years of data. Thus an update of the $X_{\max}$ anisotropy result using the Phase-I data set, reconstruction, and analysis methods is warranted.

The anisotropy test uses the Anderson-Darling two-sample homogeneity test (AD-test) [22] to compare the cumulative $X_{\max}$ distributions from the on- and off-plane regions above some energy threshold (E_{th}). Because a heavier on-plane sample was predicted, the AD-test has been modified to return a value of -2 when the $\langle X_{\max}\rangle$ of the on-plane sample is higher than that of the off-plane sample to build the test statistic (TS). To form the cumulative $X_{\max}$ distributions the energy dependence of $X_{\max}$ is removed by subtracting $\langle X_{\max}\rangle$ for iron as predicted by EPOS-LHC:

$$X'_{\max} = X_{\max} - \langle X_{\max}\rangle^{\text{EPOS}}_{\text{Fe}}. \quad (1)$$

Next, an optimization scan is performed on the data taken up until December 31$^{\text{st}}$ 2012 (46.6 % of the total data) to select the minimum threshold energy and galactic latitude cut-off, which maximize the significance of the on- and off-plane $X'_{\max}$ difference. The results of this scan can be seen in Fig. 5, where the same optimal energy and latitude thresholds, $10^{18.7}$ eV, and 30°, respectively, are found with a TS of 6.7.

The next step of the analysis chain is to check for significant differences in the $X_{\max}$ acceptance, reconstruction bias, or resolution between the on- and off-plane samples. As in earlier reports, no significant differences are found for any of these factors; however, corrections are independently parameterized and applied. The changes in the resulting magnitude due to uncertainties in these corrections are then taken as systematic uncertainties.

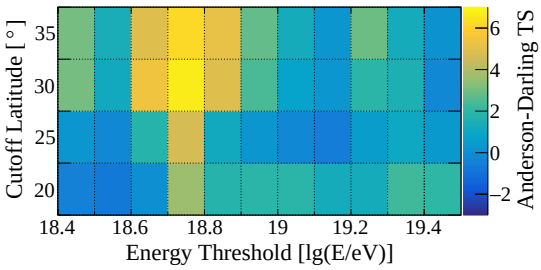

Figure 5: Parameter scan over 46.6% of the data.

At this point, a test looking for a difference in $X_{\max}$ for events arriving near and far from the galactic plane can be carried out on the blind data using the prescribed thresholds identified in the scan. The results of this test are summarized in Fig. 6 and show that with the new dataset, reconstruction methods, and atmospheric corrections, the on- and off-plane difference remains but is reduced in magnitude. With the new data and methods, the mean difference (off – on) between the integrated $X'_{\max}$ distributions is $5.1 \pm 1.5^{+2.1}_{-2.2}$ g/cm^2 while the difference in the widths is now a negligible $0.5 \pm 2.1^{+3.5}_{-2.1}$ g/cm^2. When compared to the former differences of $9.1 \pm 1.6^{+2.1}_{-2.2}$ g/cm^2 and $5.9 \pm 2.1^{+3.5}_{-2.1}$ g/cm^2 respectively, the change is substantial.

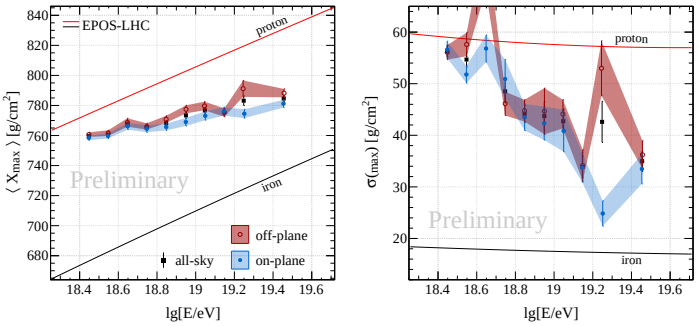

Figure 6: The first (left) and second (right) moments of the $X_{\max}$ distributions from on- and off-plane regions.

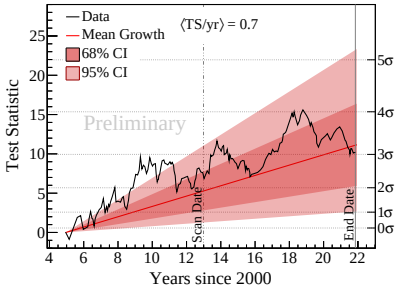

Figure 7: The time evolution of the TS with growth trend and 68 % and 95 % trend CIs. Significance indicated on the right.

With the lower overall difference in the first two moments of the on- and off-plane distributions, the TS for the blind and combined datasets are reduced now to 4.2 and 10.9, respectively. Using the same Monte Carlo methods described in [19] leads to end statistical significances of 2.7 σ for the blind data and 3.2 σ for all data. When systematic uncertainties on the mean difference and the difference in width are additionally considered, the significance of the blind data and all data results are reduced to 2.0 σ and 2.5 σ respectively.

To interpret the result and investigate what has changed from earlier reports, the composition mapping method described in [19] is used. The result of this mapping procedure produces a figure where the positive (negative) red (blue) values display that UHECR arriving from within 30° of that point have a lighter (heavier) mean mass relative to the rest of the sky. Fig. 8 shows the sky map which results from studying the Phase-I data above $10^{18.7}$ eV. In it, the excess of heavy particles along the plane is still present within 60°, however, the correlation with the galactic plane is weaker due to features at high and low galactic longitudes.

In the new Phase-I FD data, there is no longer strong support for a correlation between $X_{\max}$ and the galactic plane with the hybrid data alone. From Fig. 7, it is evident that this change is

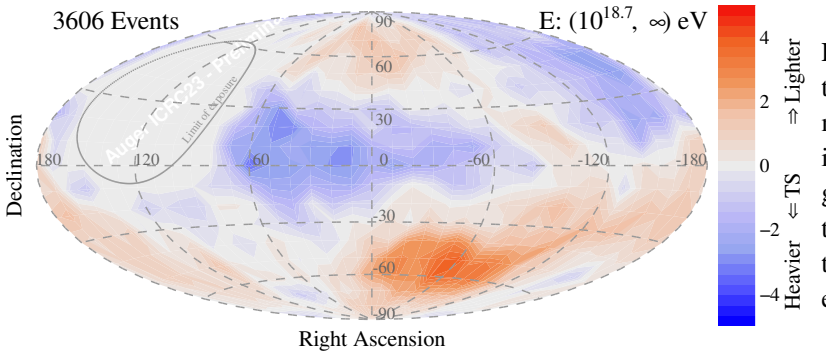

Figure 8: A map in galactic coordinates of the relative mass composition of arriving cosmic rays with energies greater than $10^{18.7}$ eV. A 30° tophat sampling is employed to gather sufficient statistics in each $5° \times 5°$ bin across the sky.

not due to an absence of the correlation in the newly collected data but rather due to an overall lowered correlation over the full breadth of the Phase-I dataset. Because there was an effect over the whole dataset, the reduction of the signal is likely sourced from the changes in the reconstruction procedures described in [20], the atmospheric corrections described in [21], or the $X_{\max}$ analysis itself [8]. One or all of these changes may have eliminated a systematic effect that was exaggerating the strength of the signal. However, the specific cause for the signal reduction is unknown at this time. Therefore the anisotropy results presented in this proceedings are preliminary pending further investigation. It is apparent from the change in results that an independent test of the result is needed to confirm or refute the anisotropy, as the current rate of signal growth will not exceed $5\,\sigma$ observation until 2035. To this end, the SD $X_{\max}$ analysis described in [9] is being prepared to test the anisotropy signal presented here and will be included in the eventual publication of this result.

Indication of a complex mass/energy evolution above 2 EeV in the phase-I SD data

As reported in [9], with its considerable statistical power, SD $X_{\max}$ can be used to reject a constant mass evolution above 3 EeV at more than $4\,\sigma$. Fig. 9 provides a coarse summary of the result, as the linear fit in the left panel is a much poorer description of the data ($\chi^2/NDF = 3.33$) than a 3-break fit to the linear-fit residuals ($\chi^2/NDF = 1.47$). Because SD $X_{\max}$ relies on the use of hadronic interaction models to train deep-learning neural networks to reconstruct $X_{\max}$, confirmation with a data-driven analysis would increase confidence in the result. The FD lacks the necessary event statistics to resolve the features. However, Δ, a parameter related to the mean risetime of SD signals, is also a mass-sensitive parameter with comparable statistics to SD $X_{\max}$ and, therefore, the energy evolution of its mean ($\langle\Delta\rangle$) may be sensitive enough to resolve the features.

A simple procedure is used to follow up the SD $X_{\max}$ result with the risetime data. First, the linear energy evolution of $\langle\delta\rangle$ is fit, and the reduced χ^2 value and residuals to the fit are extracted. Then, the residuals are fit with a 3-break broken line function with the break locations fixed to those

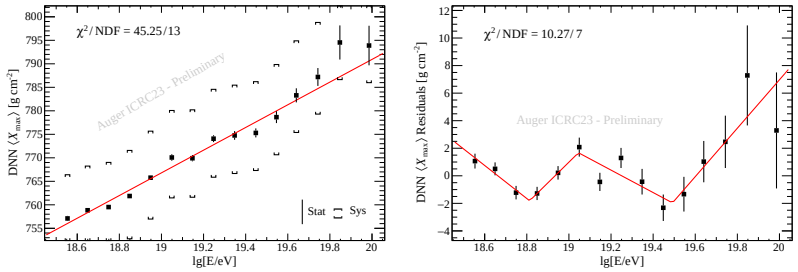

Figure 9: A linear fit to the energy evolution of SD $X_{\max}$ (left) and a broken line fit to the residuals of the fit (right). The 3-break fit is preferred. For all details, see [9].

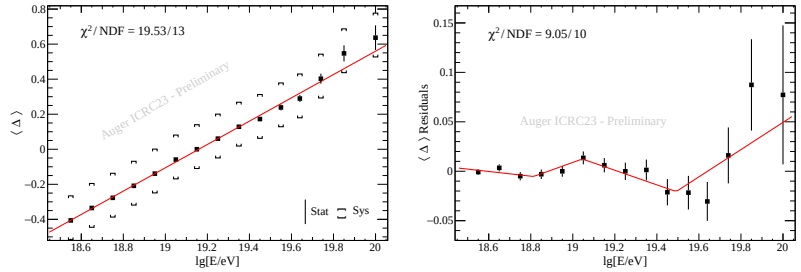

Figure 10: A linear fit to the energy evolution of $\langle\Delta\rangle$, a parameter related to the signal risetime of SD signals (left), and a broken line fit to the linear fit residuals (right). The 3-break fit is mildly preferred.

found in SD $X_{\max}$, and the reduced χ^2 value is extracted. As shown by comparing the two panes in Fig. 10, the 3-break fit produces a lower reduced χ^2 than the linear fit providing data-driven support to SD $X_{\max}$, though more in-depth studies are needed to confirm the result fully.

Discussion

After nearly two decades, the Pierre Auger Observatory has amassed the most comprehensive collection of data on UHECRs thus far assembled. Through the careful analysis of this data, the overall picture of the composition of arriving UHECRs has vastly improved. We now know that UHECRs consist of many atomic nuclei species ranging from protons to ionized iron. Their mass composition evolves strongly with energy and possibly has fine-grain features like those seen in the spectrum. The ankle is not proton-dominated, and flux trends toward heavy at the highest energies. And, while currently, no significant mass-dependent anisotropies can be claimed, there are promising hints that significant anisotropies may be resolved in the future. With these discoveries and leads combined with promising increases in mass sensitivity expected from upgraded instruments, the future looks bright for the next phase of data-taking at the Pierre Auger Observatory.

References

[1] A. Aab et al., [Pierre Auger Coll.], *Nucl. Instrum. Meth. A* **798** (2015) 172 [1502.01323].
[2] P. Abreu et al., [Pierre Auger Coll.], *JINST* **7** (2012) P10011 [1209.3840].
[3] A. Aab et al., [Pierre Auger Coll.], 1604.03637.
[4] J. Abraham et al., [Pierre Auger Coll.], *Phys. Rev. Lett.* **104** (2010) 091101 [1002.0699].
[5] A. Aab et al., [Pierre Auger Coll.], *Phys. Rev. D* **90** (2014) 122005 [1409.4809].
[6] J. Bellido, [Pierre Auger Coll.], *PoS* **ICRC2017** (2018) 506.
[7] A. Yushkov, [Pierre Auger Coll.], *PoS* **ICRC2019** (2020) 482.
[8] T. Fitoussi et al., [Pierre Auger Coll.], *PoS* **ICRC2023** (2023) 319.
[9] J. Glombitza et al., [Pierre Auger Coll.], *PoS* **ICRC2023** (2023) 278.
[10] B. Pont, [Pierre Auger Coll.], *EPJ Web Conf.* **283** (2023) 02010.
[11] A. Coleman et al., *Astropart. Phys.* **149** (2023) 102819 [2205.05845].
[12] A. Aab et al., [Pierre Auger Coll.], *Phys. Rev. D* **96** (2017) 122003 [1710.07249].
[13] A. Aab et al., [Pierre Auger Coll.], *JINST* **16** (2021) P07019 [2101.02946].
[14] S. Ostapchenko, *Phys. Rev. D* **83** (2011) 014018 [1010.1869].
[15] T. Pierog, *PoS* **ICRC2017** (2018) 1100.
[16] F. Riehn et al., *PoS* **ICRC2017** (2018) 301 [1709.07227].
[17] O. Tkachenko et al., [Pierre Auger Coll.], *PoS* **ICRC2023** (2023) 438.
[18] E. Mayotte et al., [Pierre Auger Coll.], *PoS* **ICRC2021** (2021) 321.
[19] E. Mayotte and T. Fitoussi, [Pierre Auger Coll.], *EPJ Web Conf.* **283** (2023) 03003 [2303.16336].
[20] J. Bellido et al., [Pierre Auger Coll.], *PoS* **ICRC2023** (2023) 211.
[21] V.M. Harvey et al., [Pierre Auger Coll.], *PoS* **ICRC2023** (2023) 300.
[22] T.W. Anderson and D.A. Darling, *Ann. Math. Statist.* **23** (1952) 193 .

The Pierre Auger Collaboration

A. Abdul Halim[13], P. Abreu[72], M. Aglietta[54,52], I. Allekotte[1], K. Almeida Cheminant[70], A. Almela[7,12], R. Aloisio[45,46], J. Alvarez-Muñiz[79], J. Ammerman Yebra[79], G.A. Anastasi[54,52], L. Anchordoqui[86], B. Andrada[7], S. Andringa[72], C. Aramo[50], P.R. Araújo Ferreira[42], E. Arnone[63,52], J. C. Arteaga Velázquez[67], H. Asorey[7], P. Assis[72], G. Avila[11], E. Avocone[57,46], A.M. Badescu[75], A. Bakalova[32], A. Balaceanu[73], F. Barbato[45,46], A. Bartz Mocellin[85], J.A. Bellido[13,69], C. Berat[36], M.E. Bertaina[63,52], G. Bhatta[70], M. Bianciotto[63,52], P.L. Biermann[h], V. Binet[5], K. Bismark[39,7], T. Bister[80,81], J. Biteau[37], J. Blazek[32], C. Bleve[36], J. Blümer[41], M. Boháčová[32], D. Boncioli[57,46], C. Bonifazi[8,26], L. Bonneau Arbeletche[21], N. Borodai[70], J. Brack[j], P.G. Brichetto Orchera[7], F.L. Briechle[42], A. Bueno[78], S. Buitink[15], M. Buscemi[47,61], M. Büsken[39,7], A. Bwembya[80,81], K.S. Caballero-Mora[66], S. Cabana-Freire[79], L. Caccianiga[59,49], I. Caracas[38], R. Caruso[58,47], A. Castellina[54,52], F. Catalani[18], G. Cataldi[48], L. Cazon[79], M. Cerda[10], A. Cermenati[45,46], J.A. Chinellato[21], J. Chudoba[32], L. Chytka[33], R.W. Clay[13], A.C. Cobos Cerutti[6], R. Colalillo[60,50], A. Coleman[90], M.R. Coluccia[48], R. Conceição[72], A. Condorelli[37], G. Consolati[49,55], M. Conte[56,48], F. Convenga[41], D. Correia dos Santos[28], P.J. Costa[72], C.E. Covault[84], M. Cristinziani[44], C.S. Cruz Sanchez[3], S. Dasso[4,2], K. Daumiller[41], B.R. Dawson[13], R.M. de Almeida[28], J. de Jesús[7,41], S.J. de Jong[80,81], J.R.T. de Mello Neto[26,27], I. De Mitri[45,46], J. de Oliveira[17], D. de Oliveira Franco[21], F. de Palma[56,48], V. de Souza[19], E. De Vito[56,48], A. Del Popolo[58,47], O. Deligny[34], N. Denner[32], L. Deval[41,7], A. di Matteo[52], M. Dobre[73], C. Dobrigkeit[21], J.C. D'Olivo[68], L.M. Domingues Mendes[72], J.C. dos Anjos, R.C. dos Anjos[25], J. Ebr[32], F. Ellwanger[41], M. Emam[80,81], R. Engel[39,41], I. Epicoco[56,48], M. Erdmann[42], A. Etchegoyen[7,12], C. Evoli[45,46], H. Falcke[80,82,81], J. Farmer[89], G. Farrar[88], A.C. Fauth[21], N. Fazzini[e], F. Feldbusch[40], F. Fenu[41,d], A. Fernandes[72], B. Fick[87], J.M. Figueira[7], A. Filipčič[77,76], T. Fitoussi[41], B. Flaggs[90], T. Fodran[80], T. Fujii[89,f], A. Fuster[7,12], C. Galea[80], C. Galelli[59,49], B. García[6], C. Gaudu[38], H. Gemmeke[40], F. Gesualdi[7,41], A. Gherghel-Lascu[73], P.L. Ghia[34], U. Giaccari[48], M. Giammarchi[49], J. Glombitza[42,g], F. Gobbi[10], F. Gollan[7], G. Golup[1], M. Gómez Berisso[1], P.F. Gómez Vitale[11], J.P. Gongora[11], J.M. González[1], N. González[7], I. Goos[1], D. Góra[70], A. Gorgi[54,52], M. Gottowik[79], T.D. Grubb[13], F. Guarino[60,50], G.P. Guedes[22], E. Guido[44], S. Hahn[39], P. Hamal[32], M.R. Hampel[7], P. Hansen[3], D. Harari[1], V.M. Harvey[13], A. Haungs[41], T. Hebbeker[42], C. Hojvat[e], J.R. Hörandel[80,81], P. Horvath[33], M. Hrabovský[33], T. Huege[41,15], A. Insolia[58,47], P.G. Isar[74], P. Janecek[32], J.A. Johnsen[85], J. Jurysek[32], A. Kääpä[38], K.H. Kampert[38], B. Keilhauer[41], A. Khakurdikar[80], V.V. Kizakke Covilakam[7,41], H.O. Klages[41], M. Kleifges[40], F. Knapp[39], N. Kunka[40], B.L. Lago[16], N. Langner[42], M.A. Leigui de Oliveira[24], Y Lema-Capeans[79], V. Lenok[39], A. Letessier-Selvon[35], I. Lhenry-Yvon[34], D. Lo Presti[58,47], L. Lopes[72], L. Lu[91], Q. Luce[39], J.P. Lundquist[76], A. Machado Payeras[21], M. Majercakova[32], D. Mandat[32], B.C. Manning[13], P. Mantsch[e], S. Marafico[34], F.M. Mariani[59,49], A.G. Mariazzi[3], I.C. Mariş[14], G. Marsella[61,47], D. Martello[56,48], S. Martinelli[41,7], O. Martínez Bravo[64], M.A. Martins[79], M. Mastrodicasa[57,46], H.J. Mathes[41], J. Matthews[a], G. Matthiae[62,51], E. Mayotte[85,38], S. Mayotte[85], P.O. Mazur[e], G. Medina-Tanco[68], J. Meinert[38], D. Melo[7], A. Menshikov[40], C. Merx[41], S. Michal[33], M.I. Micheletti[5], L. Miramonti[59,49], S. Mollerach[1], F. Montanet[36], L. Morejon[38], C. Morello[54,52], A.L. Müller[32], K. Mulrey[80,81], R. Mussa[52], M. Muzio[88], W.M. Namasaka[38], S. Negi[32], L. Nellen[68], K. Nguyen[87], G. Nicora[9], M. Niculescu-Oglinzanu[73], M. Niechciol[44], D. Nitz[87], D. Nosek[31], V. Novotny[31], L. Nožka[33], A Nucita[56,48], L.A. Núñez[30], C. Oliveira[19], M. Palatka[32], J. Pallotta[9], S. Panja[32], G. Parente[79], T. Paulsen[38], J. Pawlowsky[38], M. Pech[32], J. Pękala[70], R. Pelayo[65], L.A.S. Pereira[23], E.E. Pereira Martins[39,7], J. Perez Armand[20], C. Pérez Bertolli[7,41], L. Perrone[56,48], S. Petrera[45,46], C. Petrucci[57,46], T. Pierog[41], M. Pimenta[72], M. Platino[7], B. Pont[80], M. Pothast[81,80], M. Pourmohammad Shahvar[61,47], P. Privitera[89], M. Prouza[32], A. Puyleart[87], S. Querchfeld[38], J. Rautenberg[38], D. Ravignani[7], M. Reininghaus[39], J. Ridky[32], F. Riehn[79], M. Risse[44], V. Rizi[57,46], W. Rodrigues de Carvalho[80], E. Rodriguez[7,41], J. Rodriguez Rojo[11], M.J. Roncoroni[7], S. Rossoni[43], M. Roth[41], E. Roulet[1], A.C. Rovero[4], P. Ruehl[44], A. Saftoiu[73], M. Saharan[80], F. Salamida[57,46], H. Salazar[64], G. Salina[51], J.D. Sanabria Gomez[30], F. Sánchez[7], E.M. Santos[20], E. Santos[32], F. Sarazin[85], R. Sarmento[72], R. Sato[11], P. Savina[91], C.M. Schäfer[41], V. Scherini[56,48], H. Schieler[41], M. Schimassek[34], M. Schimp[38], F. Schlüter[41], D. Schmidt[39], O. Scholten[15,i], H. Schoorlemmer[80,81],

P. Schovánek[32], F.G. Schröder[90,41], J. Schulte[42], T. Schulz[41], S.J. Sciutto[3], M. Scornavacche[7,41], A. Segreto[53,47], S. Sehgal[38], S.U. Shivashankara[76], G. Sigl[43], G. Silli[7], O. Sima[73,b], F. Simon[40], R. Smau[73], R. Šmída[89], P. Sommers[k], J.F. Soriano[86], R. Squartini[10], M. Stadelmaier[32], D. Stanca[73], S. Stanič[76], J. Stasielak[70], P. Stassi[36], S. Strähnz[39], M. Straub[42], M. Suárez-Durán[14], T. Suomijärvi[37], A.D. Supanitsky[7], Z. Svozilikova[32], Z. Szadkowski[71], A. Tapia[29], C. Taricco[63,52], C. Timmermans[81,80], O. Tkachenko[41], P. Tobiska[32], C.J. Todero Peixoto[18], B. Tomé[72], Z. Torrès[36], A. Travaini[10], P. Travnicek[32], C. Trimarelli[57,46], M. Tueros[3], M. Unger[41], L. Vaclavek[33], M. Vacula[33], J.F. Valdés Galicia[68], L. Valore[60,50], E. Varela[64], A. Vásquez-Ramírez[30], D. Veberič[41], C. Ventura[27], I.D. Vergara Quispe[3], V. Verzi[51], J. Vicha[32], J. Vink[83], J. Vlastimil[32], S. Vorobiov[76], C. Watanabe[26], A.A. Watson[c], A. Weindl[41], L. Wiencke[85], H. Wilczyński[70], D. Wittkowski[38], B. Wundheiler[7], B. Yue[38], A. Yushkov[32], O. Zapparrata[14], E. Zas[79], D. Zavrtanik[76,77], M. Zavrtanik[77,76]

———— • ————

[1] Centro Atómico Bariloche and Instituto Balseiro (CNEA-UNCuyo-CONICET), San Carlos de Bariloche, Argentina
[2] Departamento de Física and Departamento de Ciencias de la Atmósfera y los Océanos, FCEyN, Universidad de Buenos Aires and CONICET, Buenos Aires, Argentina
[3] IFLP, Universidad Nacional de La Plata and CONICET, La Plata, Argentina
[4] Instituto de Astronomía y Física del Espacio (IAFE, CONICET-UBA), Buenos Aires, Argentina
[5] Instituto de Física de Rosario (IFIR) – CONICET/U.N.R. and Facultad de Ciencias Bioquímicas y Farmacéuticas U.N.R., Rosario, Argentina
[6] Instituto de Tecnologías en Detección y Astropartículas (CNEA, CONICET, UNSAM), and Universidad Tecnológica Nacional – Facultad Regional Mendoza (CONICET/CNEA), Mendoza, Argentina
[7] Instituto de Tecnologías en Detección y Astropartículas (CNEA, CONICET, UNSAM), Buenos Aires, Argentina
[8] International Center of Advanced Studies and Instituto de Ciencias Físicas, ECyT-UNSAM and CONICET, Campus Miguelete – San Martín, Buenos Aires, Argentina
[9] Laboratorio Atmósfera – Departamento de Investigaciones en Láseres y sus Aplicaciones – UNIDEF (CITEDEF-CONICET), Argentina
[10] Observatorio Pierre Auger, Malargüe, Argentina
[11] Observatorio Pierre Auger and Comisión Nacional de Energía Atómica, Malargüe, Argentina
[12] Universidad Tecnológica Nacional – Facultad Regional Buenos Aires, Buenos Aires, Argentina
[13] University of Adelaide, Adelaide, S.A., Australia
[14] Université Libre de Bruxelles (ULB), Brussels, Belgium
[15] Vrije Universiteit Brussels, Brussels, Belgium
[16] Centro Federal de Educação Tecnológica Celso Suckow da Fonseca, Petropolis, Brazil
[17] Instituto Federal de Educação, Ciência e Tecnologia do Rio de Janeiro (IFRJ), Brazil
[18] Universidade de São Paulo, Escola de Engenharia de Lorena, Lorena, SP, Brazil
[19] Universidade de São Paulo, Instituto de Física de São Carlos, São Carlos, SP, Brazil
[20] Universidade de São Paulo, Instituto de Física, São Paulo, SP, Brazil
[21] Universidade Estadual de Campinas, IFGW, Campinas, SP, Brazil
[22] Universidade Estadual de Feira de Santana, Feira de Santana, Brazil
[23] Universidade Federal de Campina Grande, Centro de Ciencias e Tecnologia, Campina Grande, Brazil
[24] Universidade Federal do ABC, Santo André, SP, Brazil
[25] Universidade Federal do Paraná, Setor Palotina, Palotina, Brazil
[26] Universidade Federal do Rio de Janeiro, Instituto de Física, Rio de Janeiro, RJ, Brazil
[27] Universidade Federal do Rio de Janeiro (UFRJ), Observatório do Valongo, Rio de Janeiro, RJ, Brazil
[28] Universidade Federal Fluminense, EEIMVR, Volta Redonda, RJ, Brazil
[29] Universidad de Medellín, Medellín, Colombia
[30] Universidad Industrial de Santander, Bucaramanga, Colombia
[31] Charles University, Faculty of Mathematics and Physics, Institute of Particle and Nuclear Physics, Prague, Czech Republic
[32] Institute of Physics of the Czech Academy of Sciences, Prague, Czech Republic
[33] Palacky University, Olomouc, Czech Republic

[34] CNRS/IN2P3, IJCLab, Université Paris-Saclay, Orsay, France
[35] Laboratoire de Physique Nucléaire et de Hautes Energies (LPNHE), Sorbonne Université, Université de Paris, CNRS-IN2P3, Paris, France
[36] Univ. Grenoble Alpes, CNRS, Grenoble Institute of Engineering Univ. Grenoble Alpes, LPSC-IN2P3, 38000 Grenoble, France
[37] Université Paris-Saclay, CNRS/IN2P3, IJCLab, Orsay, France
[38] Bergische Universität Wuppertal, Department of Physics, Wuppertal, Germany
[39] Karlsruhe Institute of Technology (KIT), Institute for Experimental Particle Physics, Karlsruhe, Germany
[40] Karlsruhe Institute of Technology (KIT), Institut für Prozessdatenverarbeitung und Elektronik, Karlsruhe, Germany
[41] Karlsruhe Institute of Technology (KIT), Institute for Astroparticle Physics, Karlsruhe, Germany
[42] RWTH Aachen University, III. Physikalisches Institut A, Aachen, Germany
[43] Universität Hamburg, II. Institut für Theoretische Physik, Hamburg, Germany
[44] Universität Siegen, Department Physik – Experimentelle Teilchenphysik, Siegen, Germany
[45] Gran Sasso Science Institute, L'Aquila, Italy
[46] INFN Laboratori Nazionali del Gran Sasso, Assergi (L'Aquila), Italy
[47] INFN, Sezione di Catania, Catania, Italy
[48] INFN, Sezione di Lecce, Lecce, Italy
[49] INFN, Sezione di Milano, Milano, Italy
[50] INFN, Sezione di Napoli, Napoli, Italy
[51] INFN, Sezione di Roma "Tor Vergata", Roma, Italy
[52] INFN, Sezione di Torino, Torino, Italy
[53] Istituto di Astrofisica Spaziale e Fisica Cosmica di Palermo (INAF), Palermo, Italy
[54] Osservatorio Astrofisico di Torino (INAF), Torino, Italy
[55] Politecnico di Milano, Dipartimento di Scienze e Tecnologie Aerospaziali , Milano, Italy
[56] Università del Salento, Dipartimento di Matematica e Fisica "E. De Giorgi", Lecce, Italy
[57] Università dell'Aquila, Dipartimento di Scienze Fisiche e Chimiche, L'Aquila, Italy
[58] Università di Catania, Dipartimento di Fisica e Astronomia "Ettore Majorana", Catania, Italy
[59] Università di Milano, Dipartimento di Fisica, Milano, Italy
[60] Università di Napoli "Federico II", Dipartimento di Fisica "Ettore Pancini", Napoli, Italy
[61] Università di Palermo, Dipartimento di Fisica e Chimica "E. Segrè", Palermo, Italy
[62] Università di Roma "Tor Vergata", Dipartimento di Fisica, Roma, Italy
[63] Università Torino, Dipartimento di Fisica, Torino, Italy
[64] Benemérita Universidad Autónoma de Puebla, Puebla, México
[65] Unidad Profesional Interdisciplinaria en Ingeniería y Tecnologías Avanzadas del Instituto Politécnico Nacional (UPIITA-IPN), México, D.F., México
[66] Universidad Autónoma de Chiapas, Tuxtla Gutiérrez, Chiapas, México
[67] Universidad Michoacana de San Nicolás de Hidalgo, Morelia, Michoacán, México
[68] Universidad Nacional Autónoma de México, México, D.F., México
[69] Universidad Nacional de San Agustin de Arequipa, Facultad de Ciencias Naturales y Formales, Arequipa, Peru
[70] Institute of Nuclear Physics PAN, Krakow, Poland
[71] University of Łódź, Faculty of High-Energy Astrophysics,Łódź, Poland
[72] Laboratório de Instrumentação e Física Experimental de Partículas – LIP and Instituto Superior Técnico – IST, Universidade de Lisboa – UL, Lisboa, Portugal
[73] "Horia Hulubei" National Institute for Physics and Nuclear Engineering, Bucharest-Magurele, Romania
[74] Institute of Space Science, Bucharest-Magurele, Romania
[75] University Politehnica of Bucharest, Bucharest, Romania
[76] Center for Astrophysics and Cosmology (CAC), University of Nova Gorica, Nova Gorica, Slovenia
[77] Experimental Particle Physics Department, J. Stefan Institute, Ljubljana, Slovenia
[78] Universidad de Granada and C.A.F.P.E., Granada, Spain
[79] Instituto Galego de Física de Altas Enerxías (IGFAE), Universidade de Santiago de Compostela, Santiago de Compostela, Spain
[80] IMAPP, Radboud University Nijmegen, Nijmegen, The Netherlands

PoS(ICRC2023)365

[81] Nationaal Instituut voor Kernfysica en Hoge Energie Fysica (NIKHEF), Science Park, Amsterdam, The Netherlands
[82] Stichting Astronomisch Onderzoek in Nederland (ASTRON), Dwingeloo, The Netherlands
[83] Universiteit van Amsterdam, Faculty of Science, Amsterdam, The Netherlands
[84] Case Western Reserve University, Cleveland, OH, USA
[85] Colorado School of Mines, Golden, CO, USA
[86] Department of Physics and Astronomy, Lehman College, City University of New York, Bronx, NY, USA
[87] Michigan Technological University, Houghton, MI, USA
[88] New York University, New York, NY, USA
[89] University of Chicago, Enrico Fermi Institute, Chicago, IL, USA
[90] University of Delaware, Department of Physics and Astronomy, Bartol Research Institute, Newark, DE, USA
[91] University of Wisconsin-Madison, Department of Physics and WIPAC, Madison, WI, USA

—

[a] Louisiana State University, Baton Rouge, LA, USA
[b] also at University of Bucharest, Physics Department, Bucharest, Romania
[c] School of Physics and Astronomy, University of Leeds, Leeds, United Kingdom
[d] now at Agenzia Spaziale Italiana (ASI). Via del Politecnico 00133, Roma, Italy
[e] Fermi National Accelerator Laboratory, Fermilab, Batavia, IL, USA
[f] now at Graduate School of Science, Osaka Metropolitan University, Osaka, Japan
[g] now at ECAP, Erlangen, Germany
[h] Max-Planck-Institut für Radioastronomie, Bonn, Germany
[i] also at Kapteyn Institute, University of Groningen, Groningen, The Netherlands
[j] Colorado State University, Fort Collins, CO, USA
[k] Pennsylvania State University, University Park, PA, USA

Acknowledgments

The successful installation, commissioning, and operation of the Pierre Auger Observatory would not have been possible without the strong commitment and effort from the technical and administrative staff in Malargüe. We are very grateful to the following agencies and organizations for financial support:

Argentina – Comisión Nacional de Energía Atómica; Agencia Nacional de Promoción Científica y Tecnológica (ANPCyT); Consejo Nacional de Investigaciones Científicas y Técnicas (CONICET); Gobierno de la Provincia de Mendoza; Municipalidad de Malargüe; NDM Holdings and Valle Las Leñas; in gratitude for their continuing cooperation over land access; Australia – the Australian Research Council; Belgium – Fonds de la Recherche Scientifique (FNRS); Research Foundation Flanders (FWO); Brazil – Conselho Nacional de Desenvolvimento Científico e Tecnológico (CNPq); Financiadora de Estudos e Projetos (FINEP); Fundação de Amparo à Pesquisa do Estado de Rio de Janeiro (FAPERJ); São Paulo Research Foundation (FAPESP) Grants No. 2019/10151-2, No. 2010/07359-6 and No. 1999/05404-3; Ministério da Ciência, Tecnologia, Inovações e Comunicações (MCTIC); Czech Republic – Grant No. MSMT CR LTT18004, LM2015038, LM2018102, CZ.02.1.01/0.0/0.0/16_013/0001402, CZ.02.1.01/0.0/0.0/18_046/0016010 and CZ.02.1.01/0.0/0.0/17_049/0008422; France – Centre de Calcul IN2P3/CNRS; Centre National de la Recherche Scientifique (CNRS); Conseil Régional Ile-de-France; Département Physique Nucléaire et Corpusculaire (PNC-IN2P3/CNRS); Département Sciences de l'Univers (SDU-INSU/CNRS); Institut Lagrange de Paris (ILP) Grant No. LABEX ANR-10-LABX-63 within the Investissements d'Avenir Programme Grant No. ANR-11-IDEX-0004-02; Germany – Bundesministerium für Bildung und Forschung (BMBF); Deutsche Forschungsgemeinschaft (DFG); Finanzministerium Baden-Württemberg; Helmholtz Alliance for Astroparticle Physics (HAP); Helmholtz-Gemeinschaft Deutscher Forschungszentren (HGF); Ministerium für Kultur und Wissenschaft des Landes Nordrhein-Westfalen; Ministerium für Wissenschaft, Forschung und Kunst des Landes Baden-Württemberg; Italy – Istituto Nazionale di Fisica Nucleare (INFN); Istituto Nazionale di Astrofisica (INAF);Ministero dell'Universitá e della Ricerca (MUR); CETEMPS Center of Excellence; Ministero degli Affari Esteri (MAE), ICSC Centro Nazionale di Ricerca in High Performance Computing, Big Data and Quantum Computing, funded by European Union NextGenerationEU, reference code CN_00000013; México – Consejo Nacional de Ciencia y Tecnología (CONACYT) No. 167733; Universidad Nacional Autónoma de México (UNAM); PAPIIT DGAPA-UNAM; The Netherlands – Ministry of Education, Culture and Science; Netherlands Organisation for Scientific Research (NWO); Dutch national e-infrastructure with the support of SURF Cooperative; Poland – Ministry of Education and Science, grants No. DIR/WK/2018/11 and 2022/WK/12; National Science Centre,

grants No. 2016/22/M/ST9/00198, 2016/23/B/ST9/01635, 2020/39/B/ST9/01398, and 2022/45/B/ST9/02163; Portugal – Portuguese national funds and FEDER funds within Programa Operacional Factores de Competitividade through Fundação para a Ciência e a Tecnologia (COMPETE); Romania – Ministry of Research, Innovation and Digitization, CNCS-UEFISCDI, contract no. 30N/2023 under Romanian National Core Program LAPLAS VII, grant no. PN 23 21 01 02 and project number PN-III-P1-1.1-TE-2021-0924/TE57/2022, within PNCDI III; Slovenia – Slovenian Research Agency, grants P1-0031, P1-0385, I0-0033, N1-0111; Spain – Ministerio de Economía, Industria y Competitividad (FPA2017-85114-P and PID2019-104676GB-C32), Xunta de Galicia (ED431C 2017/07), Junta de Andalucía (SOMM17/6104/UGR, P18-FR-4314) Feder Funds, RENATA Red Nacional Temática de Astropartículas (FPA2015-68783-REDT) and María de Maeztu Unit of Excellence (MDM-2016-0692); USA – Department of Energy, Contracts No. DE-AC02-07CH11359, No. DE-FR02-04ER41300, No. DE-FG02-99ER41107 and No. DE-SC0011689; National Science Foundation, Grant No. 0450696; The Grainger Foundation; Marie Curie-IRSES/EPLANET; European Particle Physics Latin American Network; and UNESCO.